

Conserved Charge Fluctuations in a Chiral Hadronic Model including Hadrons and Quarks

P. Rau^{a,b}, J. Steinheimer^c, S. Schramm^{a,b}, H. Stöcker^{a,b,d}

^a*Institut für Theoretische Physik, Goethe Universität, Max-von-Laue-Str. 1, 60438 Frankfurt am Main, Germany*

^b*Frankfurt Institute for Advanced Studies (FIAS), Ruth-Moufang-Str. 1, 60438 Frankfurt am Main, Germany*

^c*Lawrence Berkeley National Laboratory, Berkeley, CA 94720, USA*

^d*GSI Helmholtzzentrum für Schwerionenforschung GmbH, Planckstr. 1, 64291 Darmstadt, Germany*

Abstract

In this work the baryon number and strange susceptibility of second and fourth order are presented. The results at zero baryonchemical potential are obtained using a well tested chiral effective model including all known hadron degrees of freedom and additionally implementing quarks and gluons in a PNJL-like approach. Quark and baryon number susceptibilities are sensitive to the fundamental degrees of freedom in the model and signal the shift from massive hadrons to light quarks at the deconfinement transition by a sharp rise at the critical temperature. Furthermore, all susceptibilities are found to be largely suppressed by repulsive vector field interactions of the particles. In the hadronic sector vector repulsion of baryon resonances restrains fluctuations to a large amount and in the quark sector above T_c even small vector field interactions of quarks quench all fluctuations unreasonably strong. For this reason, vector field interactions for quarks have to vanish in the deconfinement limit.

Keywords: chiral effective model, QCD phase transition, conserved charge fluctuations, susceptibilities

PACS: 25.75.-q, 0.Rd, 25.75.Nq, 24.60.Ky

1. Introduction

A major objective of heavy-ion experiments as performed at the RHIC, LHC, and future experiments at the upcoming Facility for Antiproton and Ion Research (FAIR) is to study properties of strongly interacting matter, particularly characteristics of the phase transition at high temperatures and baryon densities. There are robust indications that in high-energy nuclear collisions an extremely hot and dense state of matter forms. This quark–gluon plasma (QGP) shows characteristics of a nearly perfect fluid with very low viscosity [1–4]. Lattice QCD has found this deconfinement transition from a hadron resonance gas (HRG) to a gas of quarks and gluons at zero baryonchemical potential $\mu_B = 0$ to happen at $T \approx 160$ MeV in a smooth cross-over for all thermodynamic variables [5, 6]. At finite μ_B , this phase transition is shifted to smaller temperatures [6–9], whereas the exact position, the order of the phase transition, and the potential existence of a critical endpoint in the region $\mu_B > 0$ are still subject of scientific study.

The extraction of robust observables for the phase transition from final state particles remains a major difficulty in studying the QCD phase diagram experimentally. Since average fluctuations of quantum numbers in a finite volume differ significantly between the confined and deconfined phase, fluctuations of conserved charges, such as of the net baryon number and the electric charge, are suitable indicators for the phase transition and may signal QGP formation [10, 11].

Generally, in experiments fluctuations of observables occur due to systematic uncertainties in experimental techniques in-

cluding inexact measurement processes and statistical uncertainties. Additional random fluctuations of more fundamental nature exist which can be attributed to the dynamics and thermodynamics of the system under consideration. In the microscopic limit, random density fluctuations occur in an early stage of a dynamically evolving system. In heavy-ion collisions initial event-by-event inhomogeneities arise due to randomly distributed impact parameters and colliding nucleons as well as to quantum fluctuations in the scattering cross sections [12]. Initial inhomogeneities in a thermalized system can strongly be amplified, when the system evolves through a phase transition [13–15]. At the critical temperature of a first-order phase transition, two degenerate thermal equilibria exist. When the hot system cools down through the transition, parts of the matter can remain in an unstable local minimum and due to spinodal decomposition narrowly defined regions with different thermodynamic properties can emerge. Furthermore, processes such as critical slowing down, reheating of the system, and the formation of domains can occur in a dynamical system near a critical point or when crossing a phase transition [12, 16–19].

Amplifications of fluctuations at the phase transition are likely to occur in heavy-ion collision, in which a highly excited and heated fireball (with parts of it potentially in thermal equilibrium) expands and cools down. In this dynamic process matter may cross a first or higher-order phase transition and potential clumping of matter and the impact of density fluctuations during hadronization may be recognizable in particle observables such as a possibly higher production rate of heavy fragments and of exotic nuclei. Therefore, the enhancement of (event-by-event) fluctuations may hint the creation of a

Email address: rau@th.physik.uni-frankfurt.de (P. Rau)

QGP [10, 11], hitting the critical point [12, 16, 20–22] or crossing a first-order phase transition [14, 15, 17–19]. However, no experimental indications for increased fluctuations in the transverse momentum close to the suggested region of a critical endpoint have been observed yet [23–25].

In heavy-ion experiments, fluctuations can be best studied on an event-by-event basis. Observations of fluctuations are restricted to accessible observables, such as correlations in the momenta of produced particles and fluctuations of the quantum numbers in small sub-volumes. In theoretical models assuming thermal equilibrium, fluctuations of conserved charges in defined volumes, such as electric charge, baryon number, (strange) quark number, and other quantum numbers, are known to correlate with higher-order cumulants of the partition function, so-called susceptibilities. This approach to fluctuations is widely used in particular by lattice QCD and other theoretical models for strongly interacting matter [26–30].

Relating theory considerations with experiment, in [31] it is pointed out that susceptibilities can be measured experimentally “since they can be expressed as integrals over either spatial or momentum space correlation functions. Thus, as long as one deals with susceptibilities, i.e. (co)-variances, there is a one to one mapping from lattice QCD results to heavy-ion collisions [...]. The susceptibilities can be extracted from data either by studying event-by-event fluctuations of a given quantity or by measuring and integrating the appropriate multi-particle densities [32].” This implies the comparability of experimental data to theoretical models, such as PNJL and chiral effective models.

For the outlined reasons, susceptibilities from the chiral model should signal the shift in the degrees of freedom at the phase transition due to the drop in the effective baryon masses (chiral transition) as well as the rising quark abundance above T_c (deconfinement transition). Comparing model results to lattice QCD can give insight into potential differences in the underlying degrees of freedom and to what extent this transition is driven by hadrons or quarks.

2. Chiral Effective Model

This work studies fluctuations of conserved charges at the phase transition using a unified approach to QCD matter. The effective model combines a SU(3)-flavor σ - ω model [33–36] with a PNJL-type approach for deconfinement [37–43]. The model features a chiral and deconfinement transition and includes both a HRG phase with the spectrum of all known hadrons with masses $m_H \leq 2.6$ GeV [44, 45] as well as a quark-gluon phase at high temperatures and densities. In the following, basic concepts of the model are shortly outlined; see [46] for a comprehensive review and all parameter values.

In mean field approximation [47, 48] the full Lagrangian reads $\mathcal{L} = \mathcal{L}_{\text{kin}} + \mathcal{L}_{\text{int}} + \mathcal{L}_{\text{mes}}$. It includes the kinetic energy of the hadrons \mathcal{L}_{kin} [35]. Furthermore, \mathcal{L}_{int} describes the attractive interaction of baryons and quarks with the scalar isoscalar mesons condensates σ , ζ and the repulsive interaction with the vector isoscalar fields ω , ϕ expressed by

$$\mathcal{L}_{\text{int}} = - \sum_i \bar{\psi}_i \left[\gamma_0 (g_{i\omega}\omega^0 + g_{i\phi}\phi^0) + m_i^* \right] \psi_i. \quad (1)$$

Index i runs over the three lightest quark flavors (u , d , s), the baryon octet, decuplet, and all heavier baryon resonances. The σ -field is the order parameter for the chiral transition.

Except for a small explicit mass δm_i , the particles’ coupling strengths $g_{i\sigma,\zeta}$ to the scalar fields dynamically generate the effective masses

$$m_i^* = g_{i\sigma}\sigma + g_{i\zeta}\zeta + \delta m_i. \quad (2)$$

It is $\delta m_{u,d} = 6$ MeV, $\delta m_s = 105$ MeV for the quarks and $\delta m_i = 150$ MeV for nucleons. The value of δm_i becomes larger with increasing vacuum mass of the specific particle. A decreasing σ -field at high T and μ causes the effective baryon masses to drop and, thus, chiral symmetry to be restored. Accordingly, the effective chemical potentials for quarks and baryons $\mu_i^* = \mu_i - g_{i\omega}\omega - g_{i\phi}\phi$, are generated by the vector couplings $g_{i\omega,\phi}$.

Couplings of the baryon octet are fixed such as to reproduce well-known vacuum masses, nuclear saturation properties, and the asymmetry energy [36, 49], resulting in $g_{\sigma}^N = -9.83$, $g_{\zeta}^N = -1.22$, $g_{\omega}^N = 11.56$ for the nucleons. Quark couplings $g_{\sigma}^{u,d} = -3.5$ for non-strange quarks and $g_{\sigma}^s = -3.5$ for strange quarks are fixed such as to restrain free quarks from the ground state and to comply with the additive quark model. The quark vector couplings g_{qv} , i.e. $g_{\omega}^{u,d}$ and g_{ϕ}^s , remain free parameters to study the repulsive effect of vector field interactions.

The baryon resonance couplings (including the decuplet) are scaled by r_s , r_v to the respective couplings of the nucleons via $g_{B_i\sigma,\zeta} = r_s \cdot g_{N\sigma,\zeta}$ and $g_{B_i\omega,\phi} = r_v \cdot g_{N\omega,\phi}$ [50]. To obtain a cross-over at $\mu_B = 0$ in all quantities, the scalar resonance coupling is fixed $r_s \approx 1$. The vector coupling r_v is varied in order to study the suppressive effect of vector field interactions. Baryon resonances have large impact on the overall phase structure and the resulting order and position of the phase transition. Reasonably large resonance vector couplings rule out a potential first-order phase transition in favor for a smooth cross-over in the whole T - μ plane [50]. This smooth transition is due to the gradual population of heavy-mass resonances states. A non-interacting HRG is considered by neglecting all particle interactions with the fields and setting δm_i to the respective vacuum mass.

The meson part of the full model Lagrangian

$$\begin{aligned} \mathcal{L}_{\text{mes}} = & \frac{1}{2} \frac{\chi}{\chi_0} \left(m_{\omega}^2 \omega^2 + m_{\phi}^2 \phi^2 \right) \\ & + g_4 \left(\omega^4 + \frac{\phi^4}{4} + 3\omega^2\phi^2 + \frac{4\omega^3\phi}{\sqrt{2}} + \frac{2\omega\phi^3}{\sqrt{2}} \right) \\ & - \frac{1}{2} k_0' (\sigma^2 + \zeta^2) + k_1 (\sigma^2 + \zeta^2)^2 \\ & + k_2 \left(\frac{\sigma^4}{2} + \zeta^4 \right) + k_3 \sigma^2 \zeta \\ & - k_4 \chi^4 - \frac{1}{4} \chi^4 \ln \frac{\chi^4}{\chi_0^4} + \frac{\delta}{3} \chi^4 \ln \frac{\sigma^2 \zeta}{\sigma_0^2 \zeta_0} \\ & - \frac{\chi^2}{\chi_0^2} \left[m_{\pi}^2 f_{\pi} \sigma + \left(\sqrt{2} m_k^2 f_k - \frac{1}{\sqrt{2}} m_{\pi}^2 f_{\pi} \right) \zeta \right] \end{aligned} \quad (3)$$

includes the mass terms, self interactions of the vector and scalar mesons, and explicit symmetry breaking. In the absence

of quarks, the dilaton field χ , introduced as a gluon condensate in order to ensure QCD scale invariance [35], is fixed at its ground state value χ_0 . In order to suppress the chiral condensate in the deconfined quark phase, a coupling of the Polyakov loop Φ to the dilaton field is introduced via

$$\chi = \chi_0 \left[1 - 1/4 (\Phi^2 + \bar{\Phi}^2)^2 \right]. \quad (4)$$

All thermodynamic quantities are derived from the grand canonical potential

$$\Omega/V = -\mathcal{L}_{\text{int}} - \mathcal{L}_{\text{mes}} + \Omega_{\text{th}}/V - U_{\text{Pol}}, \quad (5)$$

with Ω_{th} defined in the heat bath of hadrons and quarks including thermal contributions from mesons, baryons, and quarks

$$\begin{aligned} \Omega_{\text{q}\bar{\text{q}}} = & -T \sum_j \frac{\gamma_j}{(2\pi)^3} \int d^3k \left(\ln \left[1 + \Phi e^{-\frac{1}{T}(E_j^*(k) - \mu_j^*)} \right] \right. \\ & \left. + \ln \left[1 + \bar{\Phi} e^{-\frac{1}{T}(E_j^*(k) + \mu_j^*)} \right] \right), \end{aligned} \quad (6)$$

with $j = u, d, s$, the spin-isospin degeneracy factor γ_j , and the single particle energy $E_j^*(k) = \sqrt{k^2 + m_j^{*2}}$.

Quarks are introduced in the style of recent PNJL models [37–43] defining the scalar Polyakov loop field Φ via the trace of the time component A_0 of the SU(3) color gauge background field $\Phi = 1/3 \text{Tr}[\exp(-A_0/T)]$. In the heavy-quark limit, Φ signals the breakdown of Z(3) center symmetry and serves as an order parameter for deconfinement. The transition dynamics from the HRG to the deconfined quark-gluon phase are controlled by the effective Polyakov loop potential

$$\begin{aligned} U = & -\left(a(T)\bar{\Phi}\Phi \right)/2 + b(T_0/T)^3 \ln \left[1 - 6\bar{\Phi}\Phi \right. \\ & \left. + 4(\bar{\Phi}^3 + \Phi^3) - 3(\bar{\Phi}\Phi)^2 \right], \end{aligned} \quad (7)$$

adopted from [42]. Together with the parameter $a(T) = a_0 + a_1(T_0/T) + a_2(T_0/T)^2$ and all parameters therein (see [46] for values), $U(T, \Phi, \bar{\Phi})$ is constructed such as to reproduce lattice data for QCD thermodynamics in the pure gauge sector as well as known features of the deconfinement transition [42]. At low temperatures in the confined phase, the minimum of the potential lies at $\Phi = 0$ and it gradually shifts with higher temperatures to $\Phi \rightarrow 1$ above the critical Polyakov temperature T_0 .

Minimizing $\Omega/V(T, \mu)$ with respect to the fields, yields the equations of motion of the fields and particle densities. Solving this set of equations, all thermodynamic variables are derived from the pressure $p = -\partial\Omega/\partial V$ and the entropy density $s = \partial p/\partial T$ and the expression for the internal energy $\epsilon = Ts - pV + \sum_i \mu_i \rho_i$, where i includes all particles in the model.

With increasing temperatures, the particle density of hadrons decreases significantly leaving pure quark-gluon matter in the high-temperature limit. In the chiral model, this shift in the fundamental degrees of freedom is implemented via an eigen-volume V_{ex}^i of all hadrons i , in analogy to [51–53] and also used in similar hadron models [54–58]. The baryons exhibit a volume V_{ex}^B close to the proton charge volume [59] and the

mesons $V_{\text{ex}}^M = 1/8 V_{\text{ex}}^B$. Since quarks are assumed to be point-like $V_{\text{ex}}^q = 0$. This formalism ensures an effective suppression of hadrons at high T and μ , at the latest when quark abundances rise quickly at the deconfinement phase transition, and in the high- T , high- μ limit a pure quark-gluon phase is established. In order not to spoil the model's thermodynamic consistency, the introduction of an excluded volume entails the re-definition of the chemical potentials, i.e. reducing μ_i^* by the occupied volume as shown in [46]. Furthermore, the particle densities as well as the energy and the entropy have to be corrected by the ratio of the total volume to the non-occupied sub-volume.

2.1. Susceptibilities

At any given point in the phase diagram (T, μ_B) , the pressure $p(T, \mu_B)$ can be determined by Taylor expanding the pressure at T and zero baryonchemical potential $p(T, \mu_B = 0) = -\Omega/V$ with respect to the ratio μ_B/T

$$\frac{p(T, \mu_B)}{T^4} = \sum_{n=0}^{\infty} c_n^B(T) \left(\frac{\mu_B}{T} \right)^n. \quad (8)$$

In the limit of small μ_B , this method yields good numerical results and is widely used by lattice QCD for the extrapolation of data at $\mu_B \neq 0$ along lines of constant μ_B/T -ratio [26, 60–62]. The Taylor coefficients of the order n are defined as

$$c_n^B(T) = \frac{1}{n!} \left. \frac{\partial^n (p(T, \mu_B)/T^4)}{\partial (\mu_B/T)^n} \right|_{\mu_B=0}, \quad (9)$$

which are related to the susceptibilities χ_n^B , analogously to cumulants in classical statistics, via

$$\chi_n^B = n! c_n^B. \quad (10)$$

In general, the susceptibilities $\chi_n^{i,j,k}$ are derived from the grand canonic partition function $\mathcal{Z} = \exp(-\Omega/T)$ using

$$\chi_n^{i,j,k}(T) = \frac{1}{V T^3} \frac{\partial^n \partial^{n_i} \partial^{n_j} \partial^{n_k}}{\partial (\mu_i/T)^{n_i} \partial (\mu_j/T)^{n_j} \partial (\mu_k/T)^{n_k}} \ln(\mathcal{Z}). \quad (11)$$

The $\chi_n^{i,j,k}$ signal fluctuations of conserved charges $Q^{i,j,k}$ [63]. Considering three-flavor QCD, the conserved charges Q are baryon number B , electric charge Q and strangeness S . In the following, only B and S fluctuations are considered.

Following this procedure, the first-order strange quark susceptibility $\chi_2^S(T)$ is determined by expanding the pressure with respect to the strange chemical potential μ_s

$$\chi_2^S(T) = \left. \frac{\partial^2 (p(T, \mu_s))}{\partial \mu_s^2} \right|_{\mu_s=0}. \quad (12)$$

This quantity describes fluctuations of the strangeness quantum number at zero strange quark chemical potential.

Since in the chiral hadronic model, $p(T, \mu_B, \mu_s)$ can be calculated at any given point in the phase diagram, susceptibilities can directly be determined numerically via Eqs. (9), (12).

3. Results

In order to quantify the impact of the quark phase and of repulsive vector interactions, this study of fluctuations in the transition region compares susceptibilities with different model parameterizations differing in the fundamental particle constituents and the respective couplings strengths. The *HRG* scenario describes the pure HRG in absence of a quark phase neglecting any excluded volume effects. In this scenario, the hadron resonance gas is considered to be ideal, i.e. all hadronic degrees of freedom do not couple to the fields. Therefore, the particles' masses are fixed at their vacuum expectation values. Here, hadrons are considered to be point-like.

The interacting HRG scenario (*int. HRG*) includes only hadron degrees of freedom as well. In contrast to the HRG parametrization, in this scenario hadrons couple to the meson fields as described above. As a result, their masses and effective chemical potentials are dynamically generated. Since there is no quark phase, this parametrization also does not take into account excluded volume effects.

When implementing the PNJL-like quark phase, the *int. HRG+q* parametrization denotes the best practice scenario including hadrons and quarks fully coupled to the fields and hadrons exhibiting a finite eigenvolume.

The study of the strange susceptibility additionally makes use of the *HRG+q* parametrization. This scenario contains hadrons and quarks which are considered to be ideal, i.e. all couplings to the meson fields vanish. However, quarks still couple to Φ and excluded volume effects apply.

3.1. Non-Strange Susceptibilities

Figure 1 shows the second-order baryon number susceptibilities χ_2^B/T^2 at $\mu_B = 0$ as functions of T contrasted to lattice QCD data using different actions [29, 64, 65]. Panel (a) depicts the susceptibilities for a vanishing resonance vector coupling $r_v = 0$ and (b) for $r_v = 0.8$.

As a reference, the gray line shows the non-interacting HRG without quarks. Since this scenario lacks a phase transition, there is no shift in the underlying degrees of freedom. Hence, there is no sudden change in χ_2^B but rather it rises monotonously with increasing temperature due to the gradual population of heavy-mass resonance states. This monotonic behavior is found for both resonance vector couplings regarded here. In this scenario, the absence of suppressive vector field interactions causes an overestimation of the number of degrees of freedom entailing large χ_2^B/T^2 -values at high T .

This overestimation is even enhanced for the fully interacting HRG (red line). Considering full scalar field interactions and vanishing resonance vector couplings (a), starting from $T \approx 150$ MeV the slope of χ_2^B is much steeper than for the non-interacting HRG. This rapid rise of susceptibilities in the interacting scenario signals the sudden decline of effective baryon masses at higher T at which m^* becomes small enough for massive resonance states to be abundantly populated. In a small range around $T_c \approx 165$ MeV [50] the mass of the Δ -resonances falls down to $m_\Delta^* \approx 0.4 m_\Delta^*(T_0)$ and in the absence of a quark phase Δ -resonances become most abundant above T_c [46]. The

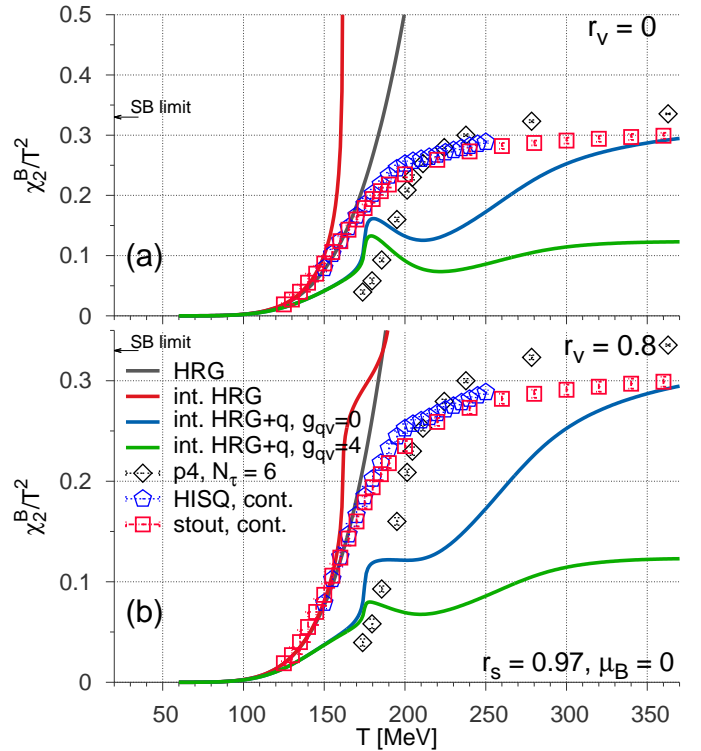


Figure 1: Second-order baryon number susceptibilities χ_2^B/T^2 at $\mu_B = 0$ as function of T . Depicted are results for resonance vector couplings $r_v = 0$ (a) and $r_v = 0.8$ (b) for the non-interacting pure HRG (gray line) and the fully interacting HRG (red line). Furthermore, results of the fully interacting model including quarks are shown for quark vector couplings $g_{qv} = 0$ (blue line) and $g_{qv} = 4.0$ (green line). The quark scalar coupling is fixed at $g_{qs} = 3.5$. Strong vector coupling suppress fluctuations significantly. Considering a finite quark vector coupling, fluctuations get unreasonably restrained above T_c . Lattice data is taken from [29] (HISQ), [64] (p4), and [65] (stout).

drop of m^* causes a sudden increase of degrees of freedom which is reflected in the steep incline of χ_2^B at T_c .

In contrast, when choosing larger and more reasonable resonance vector couplings $r_v = 0.8$ [50], hadron degrees of freedom are notably suppressed above T_c as depicted in Fig. 1 (b). With $r_v = 0.8$ the drop of m^* is still existent and χ_2^B of the int. HRG shows a sudden increase at T_c . However, at slightly higher temperatures $\chi_2^B/T^2(T)$ flattens and rises again at $T \approx 180$ MeV, where the ζ -field drops and strange baryon masses become light. In contrast, the light quark susceptibility $\chi_2^{u,d}$, which has no strange contribution, saturates at $\chi_2^{u,d}/T^2 \approx 1$ slightly above T_c . This finding underlines the major impact of hadron resonances and their couplings on the phase structure and the overall behavior of the system at T_c found in [46, 50]. The key implication of these rather large baryon resonance vector couplings lies in the disappearance of a first order phase transition and a critical end point. With $r_v \rightarrow 1$ only a smooth cross-over exists in the whole phase diagram [50].

Comparing the purely hadronic results to lattice QCD (data points corresponding to different lattice actions), the slope of $\chi_2^B/T^2(T)$ from recent continuum extrapolated lattice QCD [29, 65] is in line with HRG results of the model up to $T \approx 150$ – 170 MeV depending on the couplings. Older lattice results with

the p4 action [64] show a slightly higher T_c and seem to be too small at $T < T_c$ compared to HRG results. This discrepancy may be caused by potential cut-off effects in lattice QCD on small lattice sites ($N_\tau \leq 8$).

Similar observations for the suppression of fluctuations with stronger vector interactions are made for the fully interacting model including quarks. In the presence of a quark phase, quark vector couplings have a large effect on the χ_2^B -slope. In both panels, Fig. 1 shows results of the chiral model including quarks with vanishing quark vector couplings $g_{q\omega} = 0$ (blue line) and with finite couplings $g_{q\omega} = 4.0$ (green line), with the notation $g_{q\omega}$ and g_{qv} used synonymously. In both HRG+q scenarios the second-order susceptibilities exhibit a peak at $T_c \approx 175$ MeV when the shift in the degrees of freedom is the fastest. For higher T , susceptibilities for $g_{q\omega} = 0$ rise to the Stefan-Boltzmann (SB) limit while they saturate at much lower values in the case of $g_{q\omega} = 4.0$. At high temperatures, excluded volume effects cause an effective suppression of hadrons and result in a plateau-like slope or even a small decline of χ_2^B up to $T \approx 220$ MeV. In the presence of quarks, the effect of the resonance vector couplings on the susceptibilities lessens and when changing $r_v = 0$ (a) to $r_v = 0.8$ (b), the absolute height is only reduced by a small amount for both $g_{q\omega}$ -values.

In contrast to this rather small impact of the hadron vector couplings in the presence of a quark phase, the quark vector couplings $g_{q\omega}$ have a strong quenching effect on fluctuations. When $g_{q\omega}$ changes from zero to $g_{q\omega} = g_{N\omega}/3 = 4.0$, the height of the peak in χ_2^B decreases significantly and, likewise, the deviation from lattice data increases for $g_{q\omega} = 4.0$ at high T . In [66, 67] it is argued, that a large quark vector coupling is needed to properly describe heavy-mass neutron stars within the framework of a PNJL equation of state (EoS). This reasoning bases on the stiffening of the EoS with larger quark vector couplings [46]. Due to this substantial stiffening, the mass-radius relation for neutron stars is shifted towards higher masses, matching a constraint put up by the recent observation of massive two-solar-mass hybrid stars [68]. In stark contrast to this constraint on the EoS from neutron star properties, in the context of conserved charge fluctuations, non-vanishing quark vector couplings must be ruled out due to the strong suppression of susceptibilities above T_c . Above T_c , χ_2^B values from lattice QCD are achieved only in the full model without quark vector interactions. The suppression of fluctuations in the transition region is even more pronounced for higher-order susceptibilities.

The comparison of the Polyakov loop from the chiral model to lattice QCD as a function of the temperature [46] indicates a rather slow and smooth shift in the degrees of freedom over a large temperature-range in lattice QCD rather than a more sudden switching to quarks and gluons at T_c in PNJL models and in the chiral model. This discrepancy is underlined by the deviation of χ_2^B in the chiral model from lattice QCD. While the fully interacting HRG in the chiral model shows a sharp incline of χ_2^B at T_c , in lattice QCD the absence of a sharp rise in the susceptibilities and an increasing χ_2^B up to rather large temperatures again hint at a more gradual shift from hadrons to quarks. This immanent discrepancy between lattice QCD and

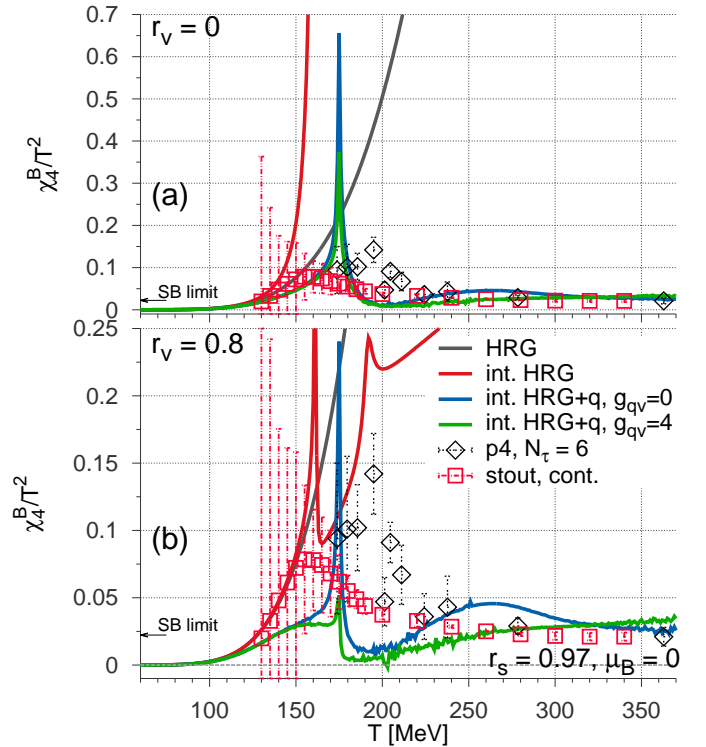


Figure 2: Fourth-order baryon number susceptibilities χ_4^B/T^2 at $\mu_B = 0$ as functions of T . The figure depicts results for two values of r_v , (a) and (b) and for the same model scenarios as in Fig. 1. Fluctuations at the phase transition decrease significantly when choosing larger vector couplings of the particles. For non-zero quark vector couplings g_{qv} (green line in (b)), χ_4^B/T^2 exhibits only a small maximum at T_c . Lattice data from [64] (p4) and [65, 70] (stout).

PNJL models in the transition to the quark sector is reflected in conserved charge fluctuations close to the critical temperature. In [69] the differences between PNJL and lattice QCD results have been attributed to the presence of bound states in the QGP even well above T_c . However, in the chiral model fluctuations above T_c are suppressed by excluded volume effects of baryons which are still present in this region.

The same conclusions as for χ_2^B also apply for higher-order susceptibilities and the impact of vector couplings on the occurrence of fluctuations close to T_c . Figure 2 shows the fourth-order susceptibilities χ_4^B/T^2 for the same model scenarios as above. As seen for χ_2^B , χ_4^B of the non-interacting HRG without quarks rises smoothly up to very high values. For the interacting HRG and $r_v = 0.8$, $\chi_4^B(T)$ exhibits a sharp peak at T_c and overestimates the susceptibilities at higher T . For $r_v = 0.8$, the contribution of strange baryons already seen in χ_2^B leads to an additional peak at $T \approx 190$ MeV. Including the quark phase with $g_{qv} = 0$ (blue line) and $r_v = 0.8$, this scenario (int. HRG+q) yields a sharp and narrow peak around T_c . In contrast, the more recent and continuum extrapolated stout data, which are derived from [65] and [70], indicate a much broader range of fluctuations which agrees with HRG results at low temperatures and reaches the quark limit at higher T . In the high-temperature limit, lattice QCD and model results including quarks converge to the SB limit.

As for χ_2^B , a larger g_{qv} strongly suppresses fluctuations.

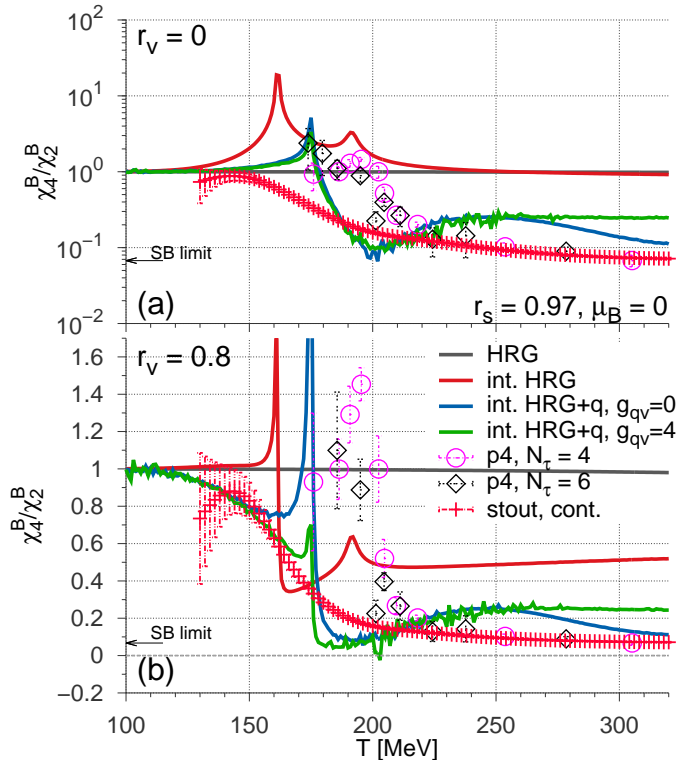


Figure 3: Ratio of the fourth to the second-order baryon number susceptibilities χ_4^B/χ_2^B at $\mu_B = 0$ as functions of T . As before, the figure illustrates results for two resonance vector couplings $r_v = 0$ (a) and $r_v = 0.8$ (b) and for model scenarios as in Fig. 1. Lattice data taken from [64] (p4) and [70] (stout).

When assuming $g_{q\omega} = 4.0$, the resulting $\chi_4^B(T)$ shows only a minor peak at T_c . This confirms the observation, that $g_{q\omega}$ has to vanish in order to reproduce fluctuations as determined by lattice QCD. In contrast to χ_2^B , χ_4^B -values from both int. HRG+q scenarios yield similar values in the high- T limit.

In heavy-ion collisions, susceptibilities are subject to additional random fluctuations due to changing volumes of the colliding systems caused by randomly different collision geometries in each collision process. To circumvent this constraining effect and to consistently remove the impact of ever varying volumes, susceptibility ratios are studied [31]. In [71] it is shown that the ratio of fourth to second-order susceptibilities χ_4^B/χ_2^B is sensitive to the shift in the system's underlying degrees of freedom. This ratio can provide information about the constituents of a thermal medium that carries net quark number in both the HRG as well as in the quark phase.

Figure 3 shows the ratio χ_4^B/χ_2^B from the model at $\mu = 0$ as a function of T . As seen for χ_2^B and χ_4^B , the ratio signals a rapid shift in the degrees of freedom at T_c by a narrow peak for all scenarios considering full mean field interactions. Again, the effective hadron suppression via excluded volume effects as well as via resonance vector couplings for all particles have major impact on the fluctuation strength and hence, on the height of the peak at T_c . Therefore, the HRG+q scenario assuming $g_{q\omega} = 4.0$ (green line) clearly underestimates χ_4^B/χ_2^B at T_c .

None of the scenarios presented here fully reproduces χ_4^B/χ_2^B -results from lattice QCD which again show a rather narrow peak

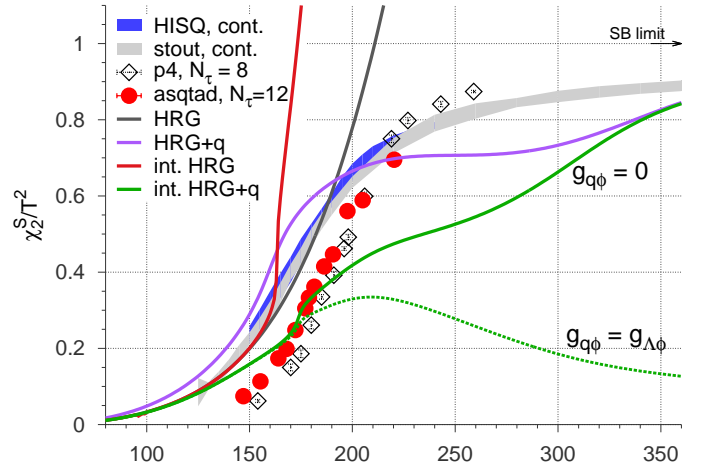


Figure 4: Strange quark number susceptibilities χ_2^S/T^2 at $\mu_B = 0$ as functions of T for the different model scenarios. The model results are contrasted to lattice data from [8, 26, 29, 65, 72–76]. Here, the resonance vector coupling is set to $r_v = 0$. When the vector coupling of the strange quark increases from $g_{q\phi} = 0$ (solid green line) to $g_{q\phi} = g_{\Lambda\phi} = -7.4$ (dashed green line), strange quark number fluctuations are notably suppressed at high T .

for older p4 and a much broader peak for recent stout results. At high temperatures $T > T_c$, effective model results with $g_{q\omega} = 0$ and lattice QCD converge again in the quark limit.

3.2. Strange Susceptibility

Below the deconfinement transition in the HRG, strangeness is carried by strange hadrons, mainly strange mesons (kaons). Compared to the temperature scale in this region, strange hadrons have rather large masses. Therefore, the production of strange hadrons is largely suppressed and their multiplicities are small at low T [46, 50]. Contrastingly, in the high- T limit, i.e. in the pure quark-gluon phase, low-mass strange quarks contribute exclusively to the total strangeness in the system. Due to the much smaller quark masses, fluctuations in the strangeness number should increase rapidly at the transition from hadrons to quarks. In the pure quark-gluon phase fluctuations of the strange quark number should reach a maximum. Due to this direct connection of strange quark number fluctuations with the underlying degrees of freedom, the strange quark susceptibility χ_2^S signaling strangeness fluctuations might serve as an indicator for the deconfinement transition (see e.g. [26, 29, 64, 65, 72, 73] for χ_2^S from lattice QCD).

Figure 4 depicts the strange susceptibility χ_2^S divided by T^2 as a function of T . Although restricting the net strangeness in the total system to $f_s = 0$, this quantity reflects the fundamental difference in underlying degrees of freedom between the different model scenarios considered here. In the non-interacting HRG, more heavy-mass strange hadrons are produced with increasing T . Since there is no abrupt shift in the degrees of freedom and the hadron masses do not change due to the absence of mean field interactions, χ_2^S rises continuously. The $\chi_2^S(T)$ reproduces lattice results up to T_c . The behavior of χ_2^S changes when m^* drops at T_c due to non-vanishing scalar field couplings. In this case (red line), with increasing T baryons lose a large amount of their mass and significantly more strange hadrons

are produced with higher T . Hence, in this case χ_2^S exhibits a steep and sudden rise at the critical temperature.

Next, this study turns to the additional quark phase and its effect on χ_2^S at the phase transition. With the HRG+q scenario neglecting all mean field interactions (purple line), the shift in the degrees of freedom is reflected by an increase of χ_2^S with a curvature qualitatively comparable to lattice results. When quarks dominate the system at temperatures above $T \approx 1.5 T_c$, χ_2^S flattens. Compared to other model scenarios, in this non-interacting HRG+q scenario χ_2^S is significantly larger at $T < T_c$. This effect can be attributed to the lack of repulsive quark interactions causing quarks to be present even at very low T and, hence, increasing strange quark fluctuations in this region. The appearance of quarks below T_c notwithstanding, it is shown in [46] that even a small quark vector couplings can prevent free quarks from populating the ground state and reasonable ground state properties can be reproduced within the effective model.

Considering the int. HRG+q scenario with full mean field interactions (green lines) the slope of $\chi_2^S(T)$ changes. Figure 4 shows results for vanishing vector couplings of the strange quarks $g_{q\phi} = 0$ (solid green line) and for a finite value $g_{q\phi} = g_{\Lambda\phi} = -7.4$ (dashed green line). For both couplings, $\chi_2^S(T)$ is much flatter as in the HRG+q scenario without interactions due to a prolonged shift from hadrons to quarks. When neglecting strange quark vector interactions $g_{q\phi} = 0$, the value of χ_2^S reaches the ideal quark gas limit (purple line) at high temperatures $T \approx 2 T_c$. Contrastingly, when strange quarks are suppressed by vector field interactions, χ_2^S reaches its maximum at T_c , where strange hadrons and quarks coexist and decreases again due to the vector suppression of strange degrees of freedom with higher temperatures.

This finding underlines the observations made for non-strange susceptibilities: Even small vector field interactions cause a significant suppression of fluctuations at the phase transition. Comparing susceptibilities from the model to lattice QCD results, it becomes apparent, that strange quarks can not exhibit a considerable coupling to the respective vector field.

When regarding the strange susceptibility as an observable for deconfinement, one should keep in mind that not only a shift from hadrons to quarks but also the drop in the effective strange-hadron masses leads to a sudden increase of χ_2^S at the critical temperature. For this reason, if the chiral and the deconfinement phase transition do not happen at the same temperature, fundamentally different and more complicated $\chi_2^S(T)$ -curves with considerable contributions both from strange hadrons and from strange quarks near the the phase transition might be possible.

4. Summary and Conclusions

This work presents non-strange and strange susceptibilities at the phase transition ($T_c \approx 165$ MeV) at $\mu_B = 0$ obtained from a chiral model including a PNJL-like quark phase. The model includes all known hadrons and quarks and by this features a chiral transition as well as deconfinement.

Comparing model results to lattice QCD, it shows that heavy-mass baryon resonances have a large effect on the hadronic sector of quark number fluctuations at T_c and the steep increase

of susceptibilities in this region results from the occurrence of multiple baryon resonance states. However, rather large repulsive vector field interactions for baryon resonances must be taken into account in order to restrain light quark number susceptibilities to values found in lattice QCD. In σ - ω models including a large spectrum of heavy-mass resonances strong vector field interactions necessarily lead to moving the critical end point to large μ_B . In the chiral model used here, vector field interactions of the size determined in this study cause the first order phase transition and a critical end point to vanish [50].

In the quark sector, model results show that particles are almost acting like an ideal gas. Particularly, this implies that repulsive interactions of quarks with strange and non-strange vector meson condensates must vanish in order not to annihilate fluctuations above T_c . The strange quark number susceptibility reflects not only the shift from hadrons to quarks but also signals a large contribution from strange baryons, which loose most of their effective masses at the chiral transition. Therefore, the strange susceptibility should not be regarded as a clear indicator for the shift in the degrees of freedom. This finding encourages further model studies to explore the contribution of hadrons and quarks at the transition using the baryon-strangeness correlator to show how fast the ideal gas limit is achieved.

5. Acknowledgements

Work was supported by BMBF, GSI, and by the Hessian excellence initiative LOEWE through the Helmholtz International Center for FAIR (HIC for FAIR), and the Helmholtz Graduate School for Hadron and Ion Research (HGS-HIRE). Computational resources were provided by the Center for Scientific Computing (CSC) of the Goethe University Frankfurt. J. S. acknowledges a Feodor Lynen fellowship of the Alexander von Humboldt foundation. The authors thank the Wuppertal-Budapest collaboration for providing recent data on c_4/c_2 and F. Karsch and the HotQCD collaboration for fruitful discussion.

References

- [1] I. Arsene et al. (BRAHMS Collab.), Nucl.Phys. **A757**, 1 (2005).
- [2] B. B. Back et al., Nucl. Phys. **A757**, 28 (2005).
- [3] J. Adams et al., Nucl. Phys. **A757**, 102 (2005).
- [4] K. Adcox et al., Nucl. Phys. **A757**, 184 (2005).
- [5] Y. Aoki, G. Endrodi, Z. Fodor, S. Katz, and K. Szabo, Nature **443**, 675 (2006).
- [6] A. Bazavov, T. Bhattacharya, M. Cheng, C. DeTar, H. Ding, et al., Phys.Rev. **D85**, 054503 (2012).
- [7] P. de Forcrand and O. Philipsen, JHEP **11**, 012 (2008).
- [8] G. Endrodi, Z. Fodor, S. Katz, and K. Szabo, JHEP **1104**, 001 (2011).
- [9] O. Kaczmarek et al., Phys. Rev. **D83**, 014504 (2011).
- [10] M. Asakawa, U. W. Heinz, and B. Muller, Phys.Rev.Lett. **85**, 2072 (2000).
- [11] S. Jeon and V. Koch, Phys.Rev.Lett. **85**, 2076 (2000).
- [12] M. A. Stephanov, K. Rajagopal, and E. V. Shuryak, Phys.Rev. **D60**, 114028 (1999).
- [13] P. Chomaz, M. Colonna, and J. Randrup, Phys.Rept. **389**, 263 (2004).
- [14] J. Steinheimer and J. Randrup, Phys.Rev.Lett. **109**, 212301 (2012).
- [15] J. Steinheimer and J. Randrup, Phys.Rev. **C87**, 054903 (2013).
- [16] M. A. Stephanov, K. Rajagopal, and E. V. Shuryak, Phys.Rev.Lett. **81**, 4816 (1998).

- [17] M. Nahrgang, S. Leupold, C. Herold, and M. Bleicher, Phys.Rev. **C84**, 024912 (2011).
- [18] C. Herold, M. Nahrgang, I. Mishustin, and M. Bleicher, Phys.Rev. **C87**, 014907 (2013).
- [19] M. Bleicher and C. Herold, PoS ConfinementX **2012**, 217 (2012).
- [20] Y. Hatta and M. Stephanov, Phys.Rev.Lett. **91**, 102003 (2003).
- [21] Y. Hatta and T. Ikeda, Phys.Rev. **D67**, 014028 (2003).
- [22] M. A. Stephanov, Prog.Theor.Phys.Suppl. **153**, 139 (2004).
- [23] J. Adams et al. (STAR Collaboration), Phys.Rev. **C71**, 064906 (2005).
- [24] K. Grebieszko, C. Alt, T. Anticic, B. Baatar, D. Barna, et al., PoS **CPOD07**, 022 (2007).
- [25] D. Adamova et al. (CERES Collaboration), Nucl.Phys. **A811**, 179 (2008).
- [26] C. Schmidt, PoS ConfinementX **2012**, 187 (2012).
- [27] V. Skokov, B. Friman, and K. Redlich (2012), arXiv:1205.4756.
- [28] K. Redlich, arXiv:1207.2610 (2012).
- [29] A. Bazavov et al. (HotQCD Collaboration), Phys.Rev. **D86**, 034509 (2012).
- [30] B. Friman, F. Karsch, K. Redlich, and V. Skokov, Eur. Phys. J. **C71**, 1694 (2011).
- [31] V. Koch (2008), arXiv:0810.2520.
- [32] A. Bialas and V. Koch, Phys.Lett. **B456**, 1 (1999).
- [33] J. Boguta and H. Stöcker, Phys.Lett. **B120**, 289 (1983).
- [34] P. Papazoglou, S. Schramm, J. Schaffner-Bielich, H. Stoecker, and W. Greiner, Phys.Rev. **C57**, 2576 (1998).
- [35] P. Papazoglou, D. Zschesche, S. Schramm, J. Schaffner-Bielich, H. Stöcker, et al., Phys.Rev. **C59**, 411 (1999).
- [36] V. Dexheimer and S. Schramm, Astrophys.J. **683**, 943 (2008).
- [37] K. Fukushima, Phys.Lett. **B591**, 277 (2003).
- [38] P. N. Meisinger and M. C. Ogilvie, Nucl.Phys.Proc.Suppl. **47**, 519 (1996).
- [39] P. N. Meisinger and M. C. Ogilvie, Phys.Lett. **B379**, 163 (1995).
- [40] C. Ratti, M. Thaler, and W. Weise, Rom.Rep.Phys. **58**, 13 (2006).
- [41] C. Ratti, M. A. Thaler, and W. Weise (2006), nucl-th/0604025.
- [42] C. Ratti, S. Roessner, M. Thaler, and W. Weise, Eur.Phys.J. **C49**, 213 (2007).
- [43] S. Roessner, C. Ratti, and W. Weise, Phys.Rev. **D75**, 034007 (2006).
- [44] J. Beringer et al. (Particle Data Group), Phys.Rev. **D86**, 010001 (2012).
- [45] K. Nakamura et al. (Particle Data Group), J.Phys. **G37**, 075021 (2010).
- [46] P. Rau, J. Steinheimer, S. Schramm, and H. Stöcker, J.Phys. **G40**, 085001 (2013).
- [47] B. D. Serot and J. D. Walecka, Adv. Nucl. Phys. **16**, 1 (1986).
- [48] B. D. Serot and J. D. Walecka, Int.J.Mod.Phys. **E6**, 515 (1997).
- [49] V. A. Dexheimer and S. Schramm, Phys.Rev. **C81**, 045201 (2009).
- [50] P. Rau, J. Steinheimer, S. Schramm, and H. Stöcker, Phys.Rev. **C85**, 025204 (2012).
- [51] D. H. Rischke, M. I. Gorenstein, H. Stöcker, and W. Greiner, Z. Phys. **C51**, 485 (1991).
- [52] M. Mishra and C. P. Singh, Phys.Rev. **C76**, 024908 (2007).
- [53] J. Steinheimer, S. Schramm, and H. Stöcker, J.Phys.G **G38**, 035001 (2011).
- [54] J. Cleymans, J. Stalnacke, M. I. Gorenstein, and E. Suhonen, Phys.Scripta **48**, 277 (1992).
- [55] B.-Q. Ma, W. Greiner, Q.-R. Zhang, and D. H. Rischke, Phys.Lett. **B315**, 29 (1993).
- [56] G. D. Yen, S.-N. Yang, M. I. Gorenstein, and W. Greiner, Phys.Rev. **C56**, 2210 (1997).
- [57] M. I. Gorenstein, A. P. Kostyuk, and Y. D. Krivenko, J.Phys., J.Phys.G **G25**, L75 (1999).
- [58] K. A. Bugaev, W. Greiner, M. I. Gorenstein, and H. Stoecker, Phys.Lett. **B485**, 121 (2000).
- [59] P. Mohr, B. Taylor, and D. Newell, *The 2010 CODATA recommended values of the fundamental physical constants (web version 6.0)*, <http://physics.nist.gov/constants> (2011).
- [60] F. Karsch, K. Redlich, and A. Tawfik, Phys.Lett. B **571**, 67 (2003).
- [61] P. Huovinen and P. Petreczky, J.Phys.Conf.Ser. **230**, 012012 (2010).
- [62] C. Schmidt, Prog.Theor.Phys.Suppl. **186**, 563 (2010).
- [63] F. Karsch, B.-J. Schaefer, M. Wagner, and J. Wambach, Phys. Lett. **B698**, 256 (2011).
- [64] M. Cheng, P. Hengde, C. Jung, F. Karsch, O. Kaczmarek, et al., Phys.Rev. **D79**, 074505 (2009).
- [65] S. Borsanyi, Z. Fodor, S. D. Katz, S. Krieg, C. Ratti, et al., JHEP **1201**, 138 (2012).
- [66] R. Lastowiecki, D. Blaschke, and J. Berdermann, Phys.Atom.Nucl. **75**, 893 (2012).
- [67] D. Blaschke, D. E. Alvarez Castillo, S. Benic, G. Contrera, and R. Lastowiecki, PoS **ConfinementX**, 249 (2012).
- [68] P. B. Demorest, T. Pennucci, S. M. Ransom, M. S. E. Roberts, and J. W. T. Hessels, Nature **467**, 1081 (2010).
- [69] C. Ratti, R. Bellwied, M. Cristoforetti, and M. Barbaro, Phys.Rev. **D85**, 014004 (2012).
- [70] S. Borsanyi, Z. Fodor, S. Katz, S. Krieg, C. Ratti, et al., Phys.Rev.Lett. **111**, 062005 (2013).
- [71] S. Ejiri, K. Redlich, and F. Karsch, Phys.Lett. **B633**, 275 (2005).
- [72] Y. Aoki, S. Borsanyi, S. Durr, Z. Fodor, S. D. Katz, et al., JHEP **0906**, 088 (2009).
- [73] S. Borsanyi et al., JHEP **1009**, 073 (2010).
- [74] A. Bazavov and P. Petreczky, J. Phys. Conf. Ser. **230**, 012014 (2010).
- [75] A. Bazavov and P. Petreczky, Phys.Part.Nucl.Lett. **8**, 860 (2011).
- [76] S. Borsanyi et al., JHEP **11**, 077 (2010).